Discoveries and timing of pulsars in NGC 6440

Vleeschower, L.; Stappers, B.W.; Bailes, M.; Barr, E.D.; Kramer, M.; Ransom, S.; Ridolfi, A.; Venkatraman Krishnan, V.; Possenti, A.; Keith, M.J.; Burgay, M.; Freire, P.C.C.; Spiewak, R.; Champion, D.J.; Bezuidenhout, M.C.; Niţu, I.C.; Chen, W.; Parthasarathy, A.; Decesar, M.E.; Buchner, S.; Stairs, I.H.; Hessels, J.W.T.

Discoveries and timing of pulsars in NGC 6440

L. Vleeschower [1]* B. W. Stappers [1] M. Bailes,[2,3] E. D. Barr [4] M. Kramer,[1,4] S. Ransom [5]
A. Ridolfi [4,6] V. Venkatraman Krishnan,[4] A. Possenti,[6] M. J. Keith,[1] M. Burgay [6] P. C. C. Freire [4]
R. Spiewak [1] D. J. Champion,[4] M. C. Bezuidenhout [1] I. C. Niţu [1] W. Chen,[4] A. Parthasarathy [4]
M. E. DeCesar,[7] S. Buchner [8] I. H. Stairs[9] and J. W. T. Hessels[10,11]

[1]*Jodrell Bank Centre for Astrophysics, Department of Physics and Astronomy, The University of Manchester, Manchester M13 9PL, UK*
[2]*Centre for Astrophysics and Supercomputing, Swinburne University of Technology, P.O. Box 218, Hawthorn, VIC 3122, Australia*
[3]*ARC Centre of Excellence for Gravitational Wave Discovery (OzGrav), Mail H29, Swinburne University of Technology, PO Box 218, Hawthorn, VIC 3122, Australia*
[4]*Max-Planck-Institut für Radioastronomie, Auf dem Hügel 69, D-53121 Bonn, Germany*
[5]*National Radio Astronomy Observatory, 520 Edgemont Rd., Charlottesville, VA 22903, USA*
[6]*INAF – Osservatorio Astronomico di Cagliari, Via della Scienza 5, I-09047 Selargius (CA), Italy*
[7]*Department of Physics and Astronomy, George Mason University, Fairfax, VA 22030, USA*
[8]*South African Radio Astronomy Observatory (SARAO), 2 Fir Street, Black River Park, Observatory, Cape Town 7925, South Africa*
[9]*Dept. of Physics and Astronomy, University of British Columbia, 6224 Agricultural Road, Vancouver, BC V6T 1Z1, Canada*
[10]*ASTRON, the Netherlands Institute for Radio Astronomy, Oude Hoogeveensedijk 4, NL-7991 PD Dwingeloo, the Netherlands*
[11]*Anton Pannekoek Institute for Astronomy, University of Amsterdam, Postbus 94249, NL-1090 GE Amsterdam, the Netherlands*

ABSTRACT

Using the MeerKAT radio telescope, a series of observations have been conducted to time the known pulsars and search for new pulsars in the globular cluster NGC 6440. As a result, two pulsars have been discovered, NGC 6440G and NGC 6440H, one of which is isolated and the other a non-eclipsing (at frequencies above 962 MHz) 'Black Widow', with a very low mass companion ($M_c > 0.006$ $M_\odot$). It joins the other binary pulsars discovered so far in this cluster that all have low companion masses ($M_c < 0.30$ $M_\odot$). We present the results of long-term timing solutions obtained using data from both Green Bank and MeerKAT telescopes for these two new pulsars and an analysis of the pulsars NGC 6440C and NGC 6440D. For the isolated pulsar NGC 6440C, we searched for planets using a Markov chain Monte Carlo technique. We find evidence for significant unmodelled variations but they cannot be well modelled as planets nor as part of a power-law red-noise process. Studies of the eclipses of the 'Redback' pulsar NGC 6440D at two different frequency bands reveal a frequency dependence with longer and asymmetric eclipses at lower frequencies (962–1283 MHz).

Key words: pulsars: individual: PSR J1748−2021C, PSR J1748−2021D, PSR J1748−2021G, PSR J1748−2021H.

1 INTRODUCTION

Globular clusters (GCs) are known to be ideal places for the production of exotic compact objects and binaries due to the high stellar densities in their cores ($\sim 10^{5-6}$ $M_\odot$ pc^{-3}; e.g. Baumgardt & Hilker 2018), which result in dynamical interactions between the stars. The exchange interactions and collisions that result in the creation or disruption of binary systems, enable the formation of, for example, cataclysmic variables or low-mass X-ray binaries (LMXBs). In fact, early observations showed that the population of LMXBs per unit mass in GCs is orders of magnitude higher than in the Galactic disc (Clark 1975; Katz 1975). LMXBs are the progenitors of millisecond pulsars (MSPs) through the recycling model (Alpar et al. 1982; Radhakrishnan & Srinivasan 1982), in which accretion on to the neutron star (NS) spins it up to millisecond periods.

The large number of LMXBs in GCs, and the detection of radio sources in the imaging of the latter, motivated surveys for radio MSPs. After the first discovery in 1987, M28A (PSR B1821–24A) by Lyne et al. (1987), 34 pulsars were soon discovered in 13 GCs which was followed by a second burst of discoveries in the 2000s thanks primarily to the Arecibo, Green Bank and Parkes telescopes (see fig. 1 from Ransom 2008) and 150 pulsars were known in 28 clusters by 2018. We have now entered a new phase. After the first searches in 2019 by the Five-hundred-meter Aperture Spherical Telescope (FAST; e.g. Pan et al. 2021) and the high gain/low system temperature MeerKAT telescope (Ridolfi et al. 2021), the number of GC pulsars has increased to 236 in at least 36 different GCs[1] up to the end of 2022 February. 32 of those new pulsars have been discovered

---

[1]See https://www3.mpifr-bonn.mpg.de/staff/pfreire/GCpsr.html for the most up-to-date GC pulsar catalogue.

*E-mail: laiila.calas@gmail.com

with FAST[2] (e.g. Pan et al. 2020, 2021; Wang et al. 2020). Both FAST and MeerKAT, one in the Northern hemisphere and the other in the Southern hemisphere, respectively, have higher sensitivity than other telescopes that have recently been used for pulsars searches in GCs. FAST, in the $-15°$ to $+65°$ declination range of the sky, has been providing a factor of 2 to 3 times better raw sensitivity than the 305-m Arecibo radio telescope (Wang et al. 2020), while MeerKAT, the precursor of the Square Kilometre Array - SKA1-mid (Dewdney et al. 2009), with a declination limit of $+44°$ (Camilo et al. 2018) is at least 3 times more sensitive than the systems used by the Parkes 64-m telescope (Stappers & Kramer 2016; Bailes et al. 2020).

A number of GCs are being searched using MeerKAT under the two Large Survey Projects: MeerTime[3] (Bailes et al. 2020) and TRAPUM[4] (TRAnsients and PUlsars with MeerKAT; Stappers & Kramer 2016), both projects collaborate together to time and search for pulsars in GCs. These searches have proven to be fruitful with the discovery of 38 new pulsars in 11 different GCs so far[5] (e.g. Ridolfi et al. 2021, 2022; Douglas et al. 2022).

NGC 6440 is a GC located at $\alpha = 17^h48^m52\overset{s}{.}84$, $\delta = -20°21'37\overset{''}{.}5$ (Pallanca et al. 2021), in the direction towards the bulge of the Galaxy at $l = 7.729°$ and $b = 3.800°$ in the constellation of Sagittarius. It is situated at a distance of 8.3 ± 0.4 kpc from the Sun (Pallanca et al. 2021) and is moderately concentrated [with a central concentration $c = 1.86$, where $c = \log(r_t/r_c)$, r_t and r_c are the tidal and core radii of the cluster, respectively] but apparently has no post-collapse core (Trager, Djorgovski & King 1993). Integrated photometry suggests that this GC was among the most metal-rich GCs in the Galaxy (Ortolani, Barbuy & Bica 1994), with its metallicity comparable to that of the Sun ([Fe/H] ~ -0.56; Origlia, Valenti & Rich 2008), and it has a reddening of $E(B - V) = 1.15$ (Valenti, Ferraro & Origlia 2007). NGC 6440 is particularly massive ($M > 4.42 \times 10^5 M_\odot$; Baumgardt & Hilker 2018) and dense with a core and half-mass radius of $r_c = 0.26$ pc and $r_h = 2.02$ pc, respectively (Pallanca et al. 2021), which corresponds to $r_c = 0.11$ arcmin and $r_h = 0.84$ arcmin.

NGC 6440 is one of the richest X-ray clusters studied so far, only surpassed by Terzan 5 (Bogdanov et al. 2021), with 25 X-ray sources within two core radii from its centre, identified by Pooley et al. (2002) and Heinke et al. (2010) using Chandra images. One of them (CX1) was later identified as a transient luminous LMXB (SAX J1748.9$-$2021) with a rotation frequency of 442 Hz (Gavriil et al. 2006, 2007). 3 yr later, a second transient LMXB (NGC 6440 X$-$2) was discovered in the cluster with coherent 206 Hz pulsations (Heinke et al. 2010), identified afterwards as an ultracompact accreting millisecond X-ray pulsar (Altamirano et al. 2010). Furthermore, the cluster is known to host six pulsars (three isolated and three binaries), with dispersion measures (DMs) between 219.4 and 227.0 pc cm^{-3} (Freire et al. 2008). Because of these characteristics, this cluster was selected as one of the high-priority targets in the Large Survey Proposals of MeerTime and TRAPUM.

The six previously known pulsars are NGC 6440A (Lyne, Manchester & D'Amico 1996) and NGC 6440B-F (Freire et al. 2008). NGC 6440A was found to be an isolated pulsar with a period of 289 ms, which is unusually long for a pulsar in a GC (Lyne et al. 1996) as only ~4 per cent of the pulsars in GCs have periods $P > 100$ ms. Almost 20 yr later, five more pulsars were discovered using the S-band receiver (1650–2250 MHz) of the Green Bank Telescope

(GBT). The other two isolated pulsars NGC 6440C and NGC 6440E have periods of 6.22 ms and 16.26 ms, respectively. NGC 6440B is a 16.7 ms pulsar in an eccentric binary system ($e = 0.57$) with an orbital period of $P_b = 20.5$ d. NGC 6440D is a Redback pulsar, i.e. an eclipsing low-mass binary, with a spin period $P = 13.49$ ms and an orbital period $P_b = 0.28$ d. It is the farthest from the GC centre as projected on the plane of the sky probably due to the formation in an exchange encounter (see Freire et al. 2008). Finally, NGC 6440F with a spin period of 3.79 ms, is at the lower end of the spin period distribution of the GC. It has an orbital period $P_b = 9.8$ d and has a white dwarf companion.

One of the most important results from Freire et al. (2008) was the measurement of the rate of advance of periastron for NGC 6440B: $\dot{\omega} = 0.00391(18)°$ yr^{-1}. Assuming that the latter is fully relativistic, this implies a total mass of $2.92 \pm 0.20 M_\odot$ (Freire et al. 2008). For an edge-on inclination ($90°$) of the orbit this gives a mass of the pulsar of $M_p = 2.3 M_\odot$. If the high inclination were confirmed, it would make it the most massive NS known so far.

In this paper, we present the discovery of two more pulsars in this cluster and a study of pulsars NGC 6440C and NGC 6440D. It is structured as follows: the observations and data reduction are described in Section 2. We report the discoveries in Section 3. The timing solutions of the pulsars discussed in this work are presented in Section 4. In Section 5, the results and their implications are summarized. Finally, the conclusions are presented in Section 6.

2 OBSERVATIONS AND DATA REDUCTION

The possibility of a very massive NS for NGC 6440B was one of the motivations for its subsequent timing (see Kramer et al. 2021). Previous observations of this pulsar made with the GBT greatly improved the precision of the measurement of $\dot{\omega}$. However, it has not been possible to obtain a significant detection of the Shapiro delay in the binary system, which suggests either a low orbital inclination or that the timing precision obtained with the GBT data was not high enough for a detection. This means that, using the GBT data alone, it was not possible to determine the individual masses of the components of the system.

Making use of the superior sensitivity of MeerKAT, a dense orbital campaign was mounted for this system with the main aim of detecting the Shapiro delay of NGC 6440B. This campaign consisted of 33 observations using the L-band (856-1712 MHz) receivers of the MeerKAT telescope (with a central frequency $f_c = 1284$ MHz) under the MeerTime project pointing towards NGC 6440B to densely sample the ~20.5-d orbit for two full revolutions. The number of antennas used for the observations depended on the orbital phase of the pulsar, with observations close to superior conjunction and periastron performed with the full array while other observations used just the central core of the array (see Table 1). This was to make sure that a number of observations had wide enough field of view to cover a significant fraction of the cluster for commensal science, given the massive time investment. Each semi-axis of the single tied-array beam (using the full array of the telescope) has a minimum size of ~0.1 arcmin at the central frequency $f_c = 1284$ MHz, covering the core radius of the GC.

We used the Pulsar Timing User Supplied Equipment (PTUSE; Bailes et al. 2020) for data acquisition. Most observations had simultaneous data acquisition on two machines, one folding NGC 6440B at the topocentric period of the pulsar and recording pulsar timing archives, while the other recording full Stokes, PSRFITS format (Hotan, van Straten & Manchester 2004) search mode filterbank data, coherently dedispersed at a DM of 220.922 pc cm^{-3},

[2] Visit the FAST GC survey https://fast.bao.ac.cn/cms/article/65/.

[3] http://www.meertime.org

[4] http://www.trapum.org

[5] See http://www.trapum.org/discoveries.html.

Table 1. Summary of the MeerKAT observations used in this analysis.

Date (yy-MM-dd-HH:mm)	Start MJD	f_c (MHz)	BW (MHz)	T_{obs} (min)	Known PSR	G Detected Y/N	H Detected Y/N	Number of Antennas
19-03-04-03:10*	58576.13	1283	321	30	B	N	N	
19-03-04-03:10*	58576.13	1444	321	30	AB	N	N	
19-07-18-18:32	58682.77	1284	642	120	ABCEF	Y	Y	57
19-07-18-20:47	58682.86	1284	642	25	ABCDE	N	Y	57
19-07-26-17:38	58690.73	1284	642	112	ABDEF	Y	Y	41
19-07-28-17:02	58692.70	1284	642	120	ABCDEF	Y	Y	59
19-07-28-19:17	58692.80	1284	642	120	ABCDEF	Y	Y	59
19-07-30-16:42	58694.69	1284	642	164	ABCDEF	Y	Y	59
19-07-30-20:30	58694.85	1284	642	163	ABCDEF	Y	Y	59
19-08-01-15:46	58696.65	1284	642	120	ABCDEF	Y	Y	58
19-08-01-18:14	58696.75	1284	642	120	ABCDEF	Y	Y	58
19-08-03-16:53	58698.70	1284	642	120	ABCDEF	Y	Y	58
19-08-03-19:12	58698.80	1284	642	120	ABCDEF	Y^s	Y	58
19-08-05-20:46	58700.86	1284	642	120	ABCDEF	Y	Y	58
19-08-05-22:59	58700.95	1284	642	120	ABCDEF	Y	Y^s	58
19-08-07-18:26	58702.76	1284	642	120	ABCDEF	Y	Y^s	42
19-08-09-17:18	58704.72	1284	642	94	ABCDEF	Y	Y	41
19-08-09-19:47	58704.82	1284	642	19	ABCDEF	N	Y	41
19-08-11-16:48	58706.70	1284	642	120	ABCDEF	Y	Y	41
19-08-11-19:22	58706.80	1284	642	120	ABCDEF	Y^s	Y	41
19-08-15-14:20	58710.59	1284	642	120	ABCDEF	Y	Y	38
19-08-15-16:41	58710.69	1284	642	120	ABCDEF	Y	Y^s	38
19-08-17-16:39	58712.69	1284	642	120	ABCDEF	Y	Y	60
19-08-17-19:11	58712.79	1284	642	120	ABCDEF	Y	Y	59
19-08-19-15:52	58714.66	1284	642	120	ABCDEF	Y	Y^s	63
19-08-19-18:11	58714.66	1284	642	120	ABCDEF	Y	Y	63
19-08-20-13:13	58715.55	1284	642	120	ABCDEF	Y^s	Y^s	63
19-08-20-15:13	58715.63	1284	642	120	ABCDEF	Y	Y^s	60
19-08-20-17:37	58715.73	1284	642	120	ABCDEF	Y^s	Y	60
19-08-20-19:37	58715.81	1284	642	120	ABCDEF	Y^s	Y	60
19-08-21-16:52	58716.70	1284	642	120	ABCDEF	Y	Y	59
19-08-25-16:43	58720.69	1284	642	180	ABCDEF	Y^s	Y	61
19-09-06-12:14	58732.50	1284	642	120	ABCDEF	Y	Y^s	60
19-09-06-14:38	58732.61	1284	642	120	ABCDEF	Y	Y	59
20-11-14-14:05^t	59167.58	1284	856	90	ABCDEF	Y	Y	60
20-11-14-15:42^t	59167.65	1284	856	143	ABCDEF	Y	Y	60
20-12-01-13:06^t	59184.54	1284	856	240	ABCDEF	Y	Y	56

*Test observation.

^{s}Pulsar found in the search.

^{t}TRAPUM observations that were used for the timing analysis of both discovered pulsars.

with 768×0.42 MHz-wide frequency channels, and a time resolution of $\sim 9.5 \mu s$. The fold mode data were used for the timing campaign whose results will be reported elsewhere (Venkatraman Krishnan et al., in preparation). The results presented in this paper used the search mode data to investigate two of the known pulsars in the GC and also to search for new pulsars. Apart from the observations performed for the timing campaign, we also analysed two other 30-min test observations taken in 2019 April with a similar set-up as above. Table 1 shows the list of observations employed in this work and includes the observing dates, the central observing frequencies f_c, the bandwidths (BW), the observation lengths T_{obs}, the known pulsars found in the search, and the number of antennas used for each of the observations. It also includes information about the detections of the two new pulsars discovered as a result of this work.

Around 75 per cent of the PTUSE data were initially analysed using the full frequency resolution and a time resolution of 76 μs (HFR). Part way through the analysis it was realised that the data volume and processing could be sped up by reducing the number of channels to 384 (LFR). This resulted in no increase in dispersion

smearing because of the initial coherent dedispersion of the data described above. The analysis was completed with the LFR data set.

All the HFR data were analysed following a typical acceleration search method. We first used the `rfifind` routine from PRESTO (Ransom, Eikenberry & Middleditch 2002) software suite to generate time–frequency masks and remove strong narrow-band and transient RFI from the data before searching. Around ∼15 per cent of the data were masked for most of the observations. We then used `prepsubband` to generate 26 dedispersed time-series from a DM of 217.00 pc cm^{-3} in steps of 0.5 pc cm^{-3}. The DM range was determined by considering ±2.5 pc cm^{-3} beyond the minimum and maximum DMs of the known pulsars in the cluster, while the DM step size was determined in order to have small DM smearing caused by an incorrect DM and sensible requirements for the processing.

A Fast Fourier Transform was applied to each of the de-dispersed time-series to obtain the power spectra; the red noise was removed from each of them using `rednoise`. Finally, the searches were carried out using `accelsearch` on the spectra, first without acceleration search ($z_{max} = 0$) and then with a z_{max} value of 200

(up to 8 harmonics), where $z = T_{obs}^2 a_l/(cP)$ is the number of Fourier bins drifted in the power spectrum (i.e. due to orbital motion) over the course of the observation, a_l is the line-of-sight acceleration due to an orbital motion, and c is the speed of light. The initial candidates were sifted using the code `accel_sift.py`.[6] The initial parameters resulting from the search for each of the candidates were used to re-fold the raw data using `prepfold`. The results were then visually inspected. We will refer to this as the PRESTO search.

The PULSAR_MINER pipeline[7] (v.1.5, see further details in Ridolfi et al. 2021) was later implemented for the searches of all the LFR observations. PULSAR_MINER automates and wraps all the processes from PRESTO's accelsearch together to facilitate the tracking of all the processes and results of the system processing, with the help of GPU acceleration (PRESTO_ON_GPU).[8] This allowed us to include a more refined search, using a DM step size of 0.05 pc cm^{-3}. We will refer to this as the PULSAR_MINER search.

The acceleration search performed by PRESTO assumes that during an observation the pulsar has a constant acceleration along the line of sight. For this reason, the algorithm might fail to find pulsars with binary orbital periods (P_b) shorter than ~10 times the duration of the observation, assuming a circular orbit (Ransom, Cordes & Eikenberry 2003). To be sensitive to orbital periods as short as ~2.5 h, we performed a 'segmented search', splitting all the observations (where possible) into sections of 60, 30, and 15 min, each of them searched individually.

The discoveries presented below motivated us to observe the cluster as part of more extensive TRAPUM searches, as the latter is capable of generating more coherent beams and so can cover more of the cluster with the full MeerKAT sensitivity. These data enabled us to better localize the two newly discovered pulsars using a close tiling of the TRAPUM beams. Covering an area of ~2 arcmin in radius, 288 coherent beams were synthesized, centred on the nominal cluster centre and using 60 antennas with a >70 per cent overlap of the synthesized beams at 1284 MHz (Chen et al. 2021). The observations had an integration time of 4 h and the data were recorded as filterbanks, with a central frequency of 1284 MHz and total intensity formed from the two orthogonal polarizations, 856 MHz of BW divided into 4096 frequency channels, with a time resolution of 76 µs. The search of these data for new pulsars is still ongoing and will be presented in a future publication. Additionally, GBT data from both the Spigot (Kaplan et al. 2005) and Green Bank Ultimate Pulsar Processing Instrument (GUPPI; DuPlain, Benson & Sessoms 2008a) backends with the L-band and S-band receivers, respectively, were used to detect the newly discovered pulsars and, hence, to obtain a long-term timing solution (see Section 4). Full details of this GBT data set can be found in Ransom et al. (in preparation).

3 DISCOVERIES

The two new MSPs discovered in NGC 6440 are described in the remainder of this section.

3.1 NGC 6440G

NGC 6440G (PSR J1748–2021G) is an isolated pulsar, with a spin period of 5.22 ms that was first found in the HFR data

from UTC 2019-08-25-16:43 in the PRESTO search at a DM of 219.719 pc cm^{-3} and with no acceleration ($z = 0$). Making use of the PULSAR_MINER search, the pulsar was subsequently found in five more observations (see Table 1). We used the best estimated period from the discoveries to fold all 33 MeerTime observations using DSPSR[9] and then optimized the period and DM using PDMP from the PSRCHIVE[10] package (Hotan et al. 2004; van Straten, Demorest & Oslowski 2012). This resulted in the detection of the pulsar in 30 out of the 33 observations that were used for the searching in this work. The non-detections are due to the short duration of the remaining observations (see Table 1).

3.2 NGC 6440H

NGC 6440H (PSR J1748–2021H) was identified as a 2.85 ms candidate in the HFR data set in the observation on 2019-08-05-22:59, but was not confirmed until we made detections in the LFR data. The non-zero acceleration and some pulse smearing observed in the diagnostic plots indicated the possibility of binary motion. We used the Period–Acceleration Diagram method (see Freire, Kramer & Lyne 2001) to obtain starting estimates of the orbital parameters. First, we measured the barycentric observed spin period P_{obs} and observed spin period derivative $\dot{P}_{obs}$ from the initial search detections. The observations with high-signal-to-noise (S/N) detections were split into two, giving us a total of six different measurements of P_{obs} and $\dot{P}_{obs}$. The $\dot{P}_{obs}$ was then converted into the line-of-sight acceleration $a_l = c(\dot{P}/P)_{obs}$. The (P_{obs}, a_l) points followed an elliptical curve indicating a circular orbit with orbital period of $P_b \simeq 8.64$ h and a projected semimajor axis of only $a_p \simeq 0.025$ lt-s.[11]

Since we have closely spaced detections, we used `fit_circular_orbit.py`[12] from PRESTO to improve the first guess values from the Period–Acceleration method. This code fits the observed spin period as a function of time, $P_{obs}(t)$, returning improved orbital parameters. The results from this fit were an orbital period of $P_b \simeq 8.66$ h and a projected semimajor axis of $a_p \simeq 0.02541$ lt-s. Those values were then further refined by phase-connecting the pulse times of arrival (ToA). The results of the timing are presented in the next section.

4 TIMING

In this section, we report the results of the timing analysis of the newly discovered pulsars as well as of NGC 6440C and NGC 6440D using data from both MeerKAT and GBT. For the case of the previously known pulsars, the MeerKAT search mode data were folded with DSPSR (van Straten & Bailes 2011) using the then best ephemeris obtained from the analysis of several years of data from the GBT. For the new discoveries, we initially used an ephemeris that included the barycentric spin period and DM of the best detection obtained with `prepfold`, and in the case of NGC 6440H, the orbital parameters from `fit_circular_orbit.py`. We then used `pat` from the PSRCHIVE package to extract the topocentric ToAs (from every archive where we detected the pulsar) by cross-correlating the pulse profiles against a noise-less template, built by fitting von Mises functions (using `paas` from PSRCHIVE) to the best-detection

[6]https://github.com/scottransom/presto/blob/master/examplescripts/ACCEL
_sift.py
[7]https://github.com/alex88ridolfi/PULSAR_MINER
[8]https://github.com/jintaoluo/presto_on_gpu

[9]http://dspsr.sourceforge.net
[10]http://psrchive.sourceforge.net/index.shtml
[11]Values obtained using the code https://github.com/lailavc/circorbit.
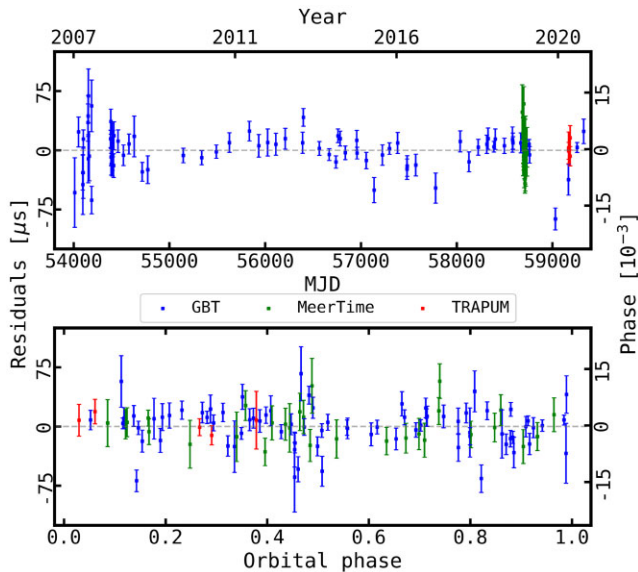[12]https://github.com/kernsuite-debian/presto/blob/master/bin/fit_circular_o
rbit.py

Figure 1. Timing residuals of NGC 6440H as a function of time (top) and orbital phase (bottom) obtained using GBT and MeerKAT data. The blue points indicate TOA from the GBT, while the green and red points show the TOA from MeerTime and TRAPUM, respectively.

Figure 2. Timing residuals of NGC 6440G as a function of time (MJD) for the GBT and MeerKAT data.

profile or one formed by adding the observations with detections, to form a mean pulse profile with higher S/N ratio. The ToAs were then referred to the Solar System Barycentre and fitted for different timing model parameters (e.g. celestial coordinates, spin parameters, and the orbital parameters in the case of the binary systems) using TEMPO2[13] (Hobbs, Edwards & Manchester 2006). The initial timing solutions for the two newly discovered pulsars were then used to fold data from the GBT to potentially extend the timing baseline to more than 14 yr.

Before 2009, the GBT data included timing observations taken using the Spigot backend (Kaplan et al. 2005) using the S-band receiver (with usable band ∼1.6–2.2 GHz). More details about these early observations can be found in Freire et al. (2008). NGC 6440 was later observed using the GUPPI (DuPlain et al. 2008b). These observations were made with both the L-band (i.e. 1.1–1.9 GHz) and S-band (i.e. 1.6–2.4 GHz, with approximately the top ∼0.7 GHz usable) receivers.

Folding the GBT data with the best ephemeris obtained from the MeerKAT data resulted in 79 detections of NGC 6440G and 77 detections of NGC 6440H. As a result, we could obtain a phase-connected timing solution extending over more than 14 yr (see Figs 1 and 2). For the case of NGC 6440G, the long-term timing solution benefitted from the localization obtained using SeeKAT (see Section 4.2.1). All the timing properties (position, proper motions, binary parameters where applicable, etc.) for the two new pulsars are presented in Table 2.

Furthermore, the GBT ToAs for NGC 6440C were combined with those from MeerKAT for further analysis and we used only MeerKAT ToAs for NGC 6440D. More details for each of the pulsars are provided in the next subsections.
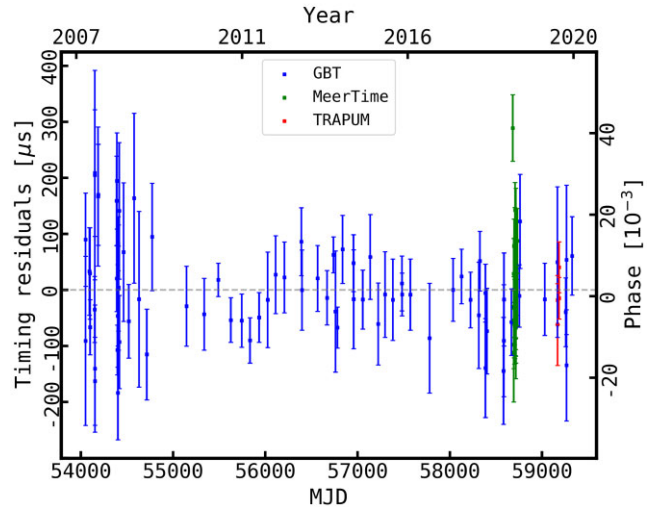
4.1 NGC 6440H

To build the timing solution for NGC 6440H we first obtained two ToAs from each of the MeerTime observations where the pulsar was detected. The ToAs were then fitted with a pulsar model containing spin (frequency and first derivative) and orbital parameters (x_p, P_b, and T_0). The initial binary parameters were derived using `fit_circular_orbit.py` as described above.

We could fold and detect the pulsar in a number of archival GBT observations of the cluster using the initial orbital model obtained with the MeerTime observations. We then used those GBT detections to generate the ToAs that were later used to obtain the long-term timing solution. For this, we first made use of the so-called jumps[14] between different epochs. This produced more refined orbital parameters, but we still needed to remove as many arbitrary jumps as possible by trying to estimate the exact number of rotations between the ToAs. We obtained a full timing solution after a few iterations of the same procedure. The minimum, median, and maximum companion mass obtained from the TEMPO2 fit were: 0.0063, 0.0072, and 0.0144 $M_\odot$, respectively, indicating that the companion is one of the lightest known. However, there is no evidence for eclipses in any of the observations, indicating that this pulsar is likely a non-eclipsing Black Widow. We were able to measure the pulsar astrometric and kinematic parameters thanks to the long timing baseline. NGC 6440H is located at RA = $17^h48^m53^s.1995(1)$, Dec. = $-20°21'35''.31(5)$ that places it 0.09 arcmin west of the cluster centre as shown in Fig. 3, which is near the edge of the core radius. The influence of the cluster on this pulsar appears to be small as the frequency derivative is about the right magnitude for an MSP (see Table 2). The proper motion is loosely constrained, with measured values of $\mu_\alpha = -0.9 \pm 0.3$ mas yr^{-1} and $\mu_\delta = -11 \pm 8$ mas yr^{-1}, these values are consistent within errors with the values reported in Vitral (2021). Fitting for the orbital period derivative, $\dot{P}_b$, we found that the uncertainty is greater than the fitted value. We also tried fitting higher orbital period derivatives but no significant values were obtained.

---

[13] https://bitbucket.org/psrsoft/tempo2/src/master/

[14] An arbitrary phase jump needed to take into account possible delays between the two different instruments.

Table 2. Timing parameters for the two new pulsars discovered in NGC 6440, as obtained from fitting the observed ToAs with TEMPO2. The companion mass is calculated assuming a pulsar mass of 1.4 $M_\odot$. For both solutions, the time units are TDB, the adopted terrestrial time standard is TT(TAI) and the Solar system ephemeris used is JPL DE421 (Folkner, Williams & Boggs 2009). Numbers in parentheses represent 1σ uncertainties in the last digit.

Pulsar	NGC 6440G	NGC 6440H
RA (J2000)	17:48:52.6460(4)	17:48:53.1995(1)
Dec. (J2000)	−20:21:40.63(1)	−20:21:35.31(5)
Proper Motion in α, μ_α (mas yr^{-1})	1.8(1.2)	−0.9(3)
Proper Motion in δ, μ_δ (mas yr^{-1})	51(32)	−11(8)
Spin Frequency, f (s^{-1})	191.742146888623(1)	351.06360053871(4)
1st Spin Frequency derivative, $\dot{f}$ (Hz s^{-2})	5.8649(3) × 10^{-15}	−2.3413(1) × 10^{-14}
2nd Spin Frequency derivative, $\ddot{f}$ (Hz s^{-2})	–	−2.04(2) × 10^{-25}
3rd Spin Frequency derivative, $\dddot{f}$ (Hz s^{-3})	–	−1.8(9) × 10^{-34}
Reference Epoch (MJD)	56668.558	56565.826
Start of Timing Data (MJD)	54050.705	54010.821
End of Timing Data (MJD)	59325.504	59184.670
DM (pc cm^{-3})	219.601(2)	222.584(7)
Number of ToAs	111	111
Weighted rms residual (μs)	68.9	17.8
S_{1300} (mJy)	0.51	0.060
L_{1300} (mJy kpc^2)	3.52	4.15
Binary parameters		
Binary Model	–	BTX
Orbital Period, P_b (d)	–	0.360787526(5)
Projected Semimajor Axis, x_p (lt-s)	–	0.025324(3)
Epoch of Ascending Node, T_{asc} (MJD)	–	58702.909365(1)
Orbital Frequency (Hz)	–	3.208002860(1) × 10^{-5}
Derived parameters		
Spin Period, P (ms)	5.2153374530685(4)	2.8484867085778(3)
1st Spin Period derivative, $\dot{P}$ (s s^{-1})	−1.59523(7) × 10^{-19}	1.89976(9) × 10^{-19}
Mass Function, $f(M_p)$ ($M_\odot$)	–	1.339(4) × 10^{-7}
Minimum companion mass, $M_{c,\,min}$ ($M_\odot$)	–	0.0063
Median companion mass, $M_{c,\,med}$ ($M_\odot$)	–	0.0072
Surface Magnetic Field†, B_0, (G)	–	7.4 × 10^8
Characteristic Age†, τ_c (Gyr)	–	2.4

†The frequency derivatives could be affected by the cluster potential and therefore affect the values of B_0 and τ_c.

4.2 NGC 6440G

GBT archival data from both the GUPPI and Spigot backends from both the L-band and S-band receivers were also folded using the initial timing solution for NGC 6440G obtained with the MeerTime data. We could not phase-connect the GBT and MeerKAT data at this point. The weak nature of the pulsar meant that an accurate localization was therefore needed. We then localized the pulsar using SeeKAT as described below. This allowed us to obtain a good enough ephemeris to fold the GBT data. After that, we obtained a timing solution of ∼14 yr using the combined GBT and MeerKAT data set (see Fig. 2) that resulted in a precise pulsar position.

4.2.1 Localization

To obtain an accurate position for the source, we used a pipeline that applies the Tied Array Beam Localisation method, known as the SeeKAT multibeam localizer[15] (Bezuidenhout et al., in preparation). This pipeline uses software called MOSAIC[16] (Chen et al. 2021) to simulate the coherent beam tiling pattern and the point spread function (PSF) of the telescope depending on the date, time, and frequency of the observation, the location where the telescopes are

[15]https://github.com/BezuidenhoutMC/SeeKAT
[16]https://gitlab.mpifr-bonn.mpg.de/wchen/Beamforming

pointing, the number of antennas used for the beamforming and the overlap fraction for placing the beams. SeeKAT uses the PSF, the coordinates (Right Ascension and Declination) and the S/N of the beams in which detections were made to determine the most likely position of the source.

In the first follow up TRAPUM observations we pointed beam number 006 (of the 288 beams in total) towards the coordinates of the MeerTime beam (which was pointed at NGC 6440B; RA = 17^{h}48^{m}52^s.95 and Dec. = −20°21′38″.90). However, the pulsar was detected with the highest S/N in TRAPUM beam number 008, with coordinates RA = 18^{h}23^{m}41^s.150 and Dec. = −30°21′38″.50, which is nearer the GC centre. To get a more accurate localization of the pulsar we used SeeKAT with both the long 2020 November observation and the 2020 December observation (see Table 1). These long observations used antennas outside of the core of the telescope and thus resulted in high-spatial resolution and good S/N. The source was detected in 4 and 7 beams in each of the observations, respectively, and the beams overlapped at 70 per cent of the maximum sensitivity. Combining all the S/Ns from all the beams with detections from both epochs, the maximum likelihood localization SeeKAT finds is RA = 17^{h}48^{m}52^s.76 ± 0.17 s, and Dec. = −20°21′38″.45 ± 2″.3, as shown in Fig. 4. The reported errors are obtained from the 2σ region, shown in lime in Fig. 4, and the maximum-likelihood position is highlighted with the cyan cross. This position places the pulsar closer to the centre of the GC ($\theta_c = 0.02$ arcmin). The long-term
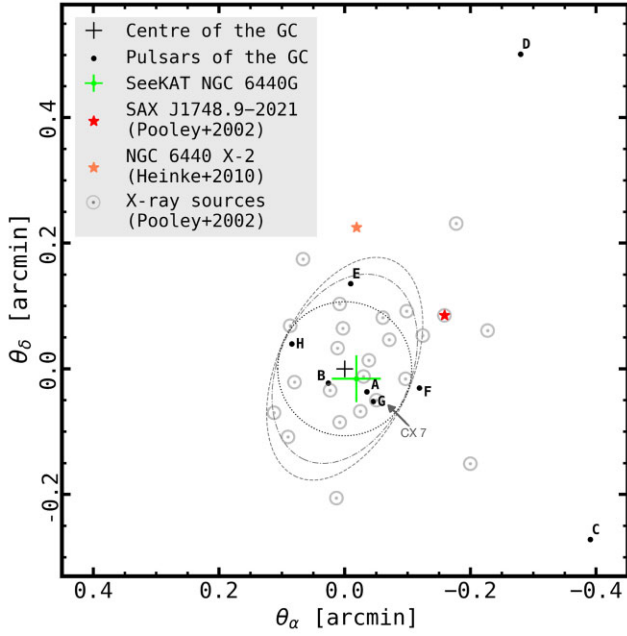
Figure 3. Positions of all the known pulsars in NGC 6440, plotted with respect to the centre of the GC. The localization of NGC 6440G is highlighted in green, the size of the symbol represents the 2σ uncertainty. The angular core radius ($r_c = 0.10$ arcmin) is indicated by the dashed circle. We show the size of the beam for 63 (inner ellipse) and 41 (outer ellipse) antennas at their 50 per cent power level. The two transient LMXBs known in the cluster are indicated with stars.

timing solution gives a position of $= 17^h48^m52\overset{s}{.}6460(4)$, and Dec. $= -20°21'40\overset{''}{.}63(1)$ which is consistent with the SeeKAT results but places the pulsar a bit further from the cluster centre, at $\theta_c = 0.07$ arcmin.

4.2.2 Proper motion

The $\sim$14-yr timing baseline provided by the GBT data allowed low-precision estimates of the proper motion of NGC 6440G, $\mu_\alpha = 1.8(1.2)$ mas yr^{-1} and $\mu_\delta = 51(32)$ mas yr^{-1}. By comparison, the proper motion of NGC 6440 has been estimated using Bayesian statistics by Vitral (2021) as $\mu_\alpha = -1.18(2)$ mas yr^{-1} and $\mu_\delta = -3.97(2)$ mas yr^{-1}, for a total proper motion of $4.14(2)$ mas yr^{-1}. Therefore, the proper motion of NGC 6440G is unlikely to be real since the source is located within the core of the GC and such a large proper motion suggests it would have left the cluster within about 130 yr. One possibility is that it recently underwent some sort of dynamical interaction, but it is unlikely given the relative time-scale.

4.2.3 Period derivative

The intrinsic period derivative of pulsars in GCs can be contaminated primarily by the acceleration of the pulsar in the gravitational field of the cluster modifying the $\dot{P}_{obs}$. In order to account for the effects that contribute to the observed period derivative $\dot{P}_{obs}$ we can use the following equation:

$$\left(\frac{\dot{P}}{P}\right)_{obs} = \left(\frac{\dot{P}}{P}\right)_{int} + \frac{a_{GC} + a_G + a_z + a_{PM}}{c}, \tag{1}$$

where $\dot{P}_{int}$ is the pulsar's intrinsic period derivative. The various types of acceleration that contribute are: the line-of-sight component
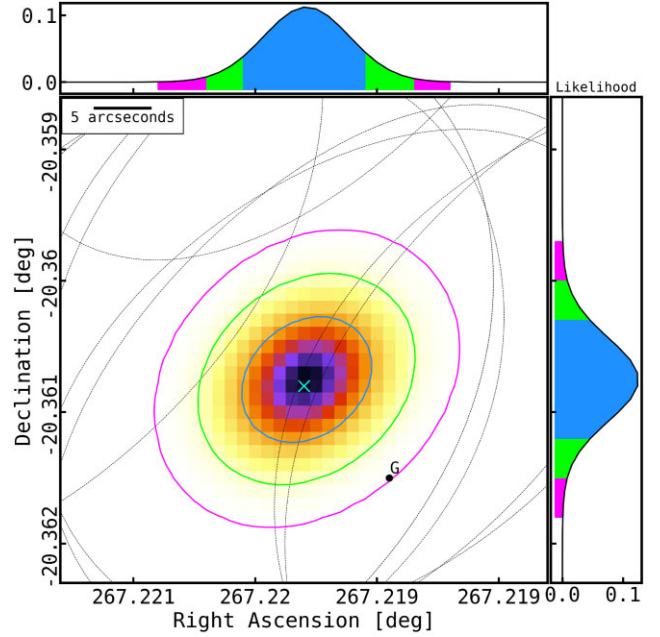

Figure 4. The localization region of NGC 6440G obtained with SeeKAT. The 1σ error region is shown in blue, and the maximum likelihood position is highlighted by the cyan cross. The 2σ and 3σ error regions are shown by the green and magenta contours, respectively. Its timing position is also shown as a dot with the letter 'G'.

of the acceleration of the pulsar caused by the gravitational field of the cluster a_{GC}, the radial acceleration due to the Galactic potential a_G, the acceleration towards the Galactic plane a_z/c, and the centrifugal acceleration due to the transverse Doppler effect (Shklovskii 1970) associated with the proper motion of the pulsar μ ($a_{PM} = \mu^2 D$, where D is the GC's distance from the Earth). The radial acceleration due to the Galactic potential is calculated using equation (2.3) in Phinney (1992), $a_G/c \approx -1.99 \times 10^{-18}$ s^{-1}. Then, using equation (4) from Nice & Taylor (1995), we derive the acceleration towards the Galactic plane, $a_z/c \approx 1.62 \times 10^{-19}$ s^{-1}. We estimate $a_{PM}/c \approx 3.44 \times 10^{-19}$ s^{-1} using the reported proper motion of NGC 6440 in Vitral (2021) and the cluster distance (see also Lazaridis et al. 2009). The measured value of $(\dot{P}/P)_{obs} = -1.49 \times 10^{-16}$ s^{-1}, is much larger than the Galactic and Shklovskii terms and so the dominant contribution must be due to the cluster.

In order to estimate the contribution from the GC potential, we consider a spherically symmetric cluster

$$\frac{a_{GC}}{c} = -\frac{l}{c}\frac{GM(<r_{psr})}{r_{psr}^3}, \tag{2}$$

where G is the gravitational constant, $r_{psr} = \sqrt{R_\perp^2 + l^2}$, is the distance from the pulsar to the centre of the cluster, $R_\perp$ is the projected distance on the sky plane between the cluster centre and the pulsar and l is the distance between the pulsar and the plane of the sky passing through the cluster centre. The mass within the radius of the pulsar is given by

$$M(<r_{psr}) = \int_0^{r_{psr}} 4\pi R^2 \rho(R) \mathrm{d}R, \tag{3}$$

where the volume mass density distribution is

$$\rho(R) = -\frac{1}{\pi}\int_R^{r_t}\frac{\mathrm{d}\Sigma(r)}{\mathrm{d}r}\frac{1}{\sqrt{r^2 - R^2}}\mathrm{d}r. \tag{4}$$
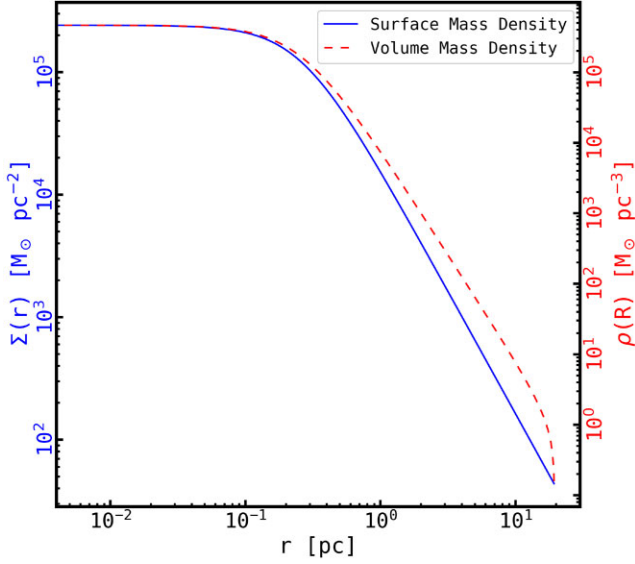
Figure 5. The surface mass density Σ as a function of the distance to the cluster centre r is shown as a blue solid line and enumerated on the left-hand side of the y-axis. The red dashed line shows the variation of the volume mass density distribution as a function of the distance r, and uses the right-hand side of the y-axis.

We use a two-parameter King model (King 1962) to describe the surface mass density

$$\Sigma(r) = \Sigma_0 \frac{1}{1 + (r/r_c)^2}, \tag{5}$$

in this case $r_c = 0.26$ pc. We can then use the cluster's total mass M_{tot} to make an estimate of the central surface mass density Σ_0 given by

$$\Sigma_0 = \frac{M_{tot}}{\int_0^{r_t} \frac{2\pi r \, dr}{1 + (r/r_c)^2}}. \tag{6}$$

Equations (2) to (6) were developed in more detail in the appendix of Freire et al. (2005).

The values $r_c = 0.26$ pc and $r_t = 19.4$ pc were obtained from the most recent measurement of the basic parameters for NGC 6440 by Pallanca et al. (2021) and $M_{tot} = 4.42 \times 10^5$ M$_\odot$ from Baumgardt & Hilker (2018). The resulting $\Sigma_0 \approx 2.41 \times 10^5$ M$_\odot$ pc^{-2} is then substituted to equation (5) to give us the surface mass density. The resulting variation of the volume mass density $\rho(R)$ as a function of the distance r to the centre of the cluster is shown in Fig. 5.

We can use the volume mass density to calculate the mass within the radius of the pulsar (equation 3). However, since r_{psr} cannot be directly measured, we used $R_\perp = 0.16$ pc (see Table 4). We estimate the mass within the radius of NGC 6440G to be $M(< r_{psr}) \approx 6.6 \times 10^3$ M$_\odot$. We use this value to determine a_{GC}/c as a function of l (see Fig. 6).

Since we do not know the exact value of l, we can calculate the maximum acceleration expected near the GC centre ($R_\perp < 2r_c$, within ~ 50 per cent) by using equation (2.7) from Phinney (1992). Since we do not have an accurate value of the line-of-sight velocity dispersion at the pulsar position $v_l^2(R_\perp)$, we use the value of the velocity dispersion of the cluster core $v_z(0)$ assuming that the dispersion does not change significantly at our small distance from the core. We take the value $v_z(0) = 13.01$ km s^{-1} from Webbink (1985), and as a result we estimate $|a_{GC}|/c = 8.94 \times 10^{-17}$ s^{-1}. This value is of the same order of magnitude to the observed value
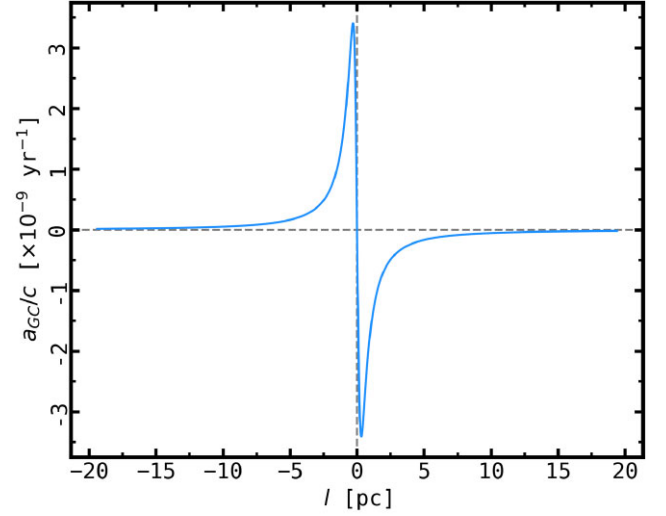

Figure 6. The line-of-sight acceleration due to the potential of the cluster as a function of the distance between the pulsar and the plane of the sky passing through the cluster centre l for a measured $R_\perp$.

of $|\dot{P}/P| = 3.05 \times 10^{-17}$ s^{-1}, which agrees with our assertion that the observed period derivative is dominated by acceleration in the cluster. The negative value of the $(\dot{P}/P)_{obs}$ indicates that it is on the back side of the cluster, but close to the centre (see Fig. 6). For comparison, we calculate the absolute upper limit on the acceleration $a_{GC,max}$ and the maximum intrinsic period derivative $\dot{P}_{int}$ for all the pulsars studied in this work (see Table 3).

4.3 Possible counterparts and location in the cluster

Fig. 3 shows the positions of all the known pulsars in the cluster relative to its centre. We also show the positions of the known X-ray sources in this GC as grey dots, and the grey circles show their positional uncertainty (from Pooley et al. 2002). Using our best position we find that NGC 6440G is potentially associated with source CX 7 in Pooley et al. (2002). The positional offset is 0.32 arcsec and the uncertainty is 1.3 arcsec. CX 7 has an X-ray luminosity of $L_X = 2.0 \times 10^{32}$ (± 21 per cent) erg s^{-1}. Using the observed relation $L_X \approx 10^{-3} L_{sd}$, where $L_{sd} \equiv I(2\pi)^2 \dot{P}/P^3$ is the spin-down luminosity of the pulsar (Verbunt et al. 1996), this implies an $L_{sd} \sim 10^{35}$ erg s^{-1}. Then, if the sources are associated, the period derivative of the pulsar should be of the order of $\sim 10^{-19}$ s s^{-1}.

In Table 4, we report the angular offsets of all the pulsar positions relative to the centre of the GC. The projected distances ($R_\perp$) were calculated using the most recent GC parameters from Pallanca et al. (2021). The positions of the known pulsars were obtained from Freire et al. (2008). We note that the two pulsars discovered in this work are located within the core radius of the GC.

4.4 Flux densities

The flux densities at ~ 1300 MHz (S_{1300}) of the new pulsars and their pseudo-luminosities ($L_{1300} \equiv S_{1300} D^2$) are calculated using the radiometer equation (Dewey et al. 1985) and using the cluster distance from Pallanca et al. (2021). To calculate the system equivalent flux density at 1300 MHz, we used a system temperature $T_{sys} = 26$ K, which includes the atmosphere plus the ground spillover

Table 3. Limits for derived parameters of the pulsars in NGC 6440 studied in this paper.

Pulsar	P (ms)	$\dot{P}_{\rm obs}$ (10^{-18})	$a_{\rm p,max}$ $(10^{-9}\,{\rm m\,s^{-2}})$	$a_{\rm GC,max}$ $(10^{-9}\,{\rm m\,s^{-2}})$	$\dot{P}_{\rm int,max}$ (10^{-18})	$B_{\rm max}$ $(10^{9}\,{\rm G})$	$\tau_{\rm c,\,min}$ (Gyr)
C	6.2269328180(7)	$-0.062(2)$	-2.89	6.99	0.08	0.74	1.15
D	13.495818491(3)	0.558678(16)	13.03	5.83	0.85	3.43	0.25
G	5.2153374530685(4)	$-1.59523(7)$	-9.17	26.80	0.31	1.28	0.27
H	2.8484867085591(7)	1.89958(3)	20.00	24.15	0.42	1.10	0.10

Table 4. Pulsar offsets from the centre of NGC 6440.

			$\theta_\perp$		
Pulsar	θ_α^* (arcmin)	θ_δ^* (arcmin)	(arcmin)	(θ_c)	$r_\perp$ (pc)
A	-0.0354	-0.0366	0.05	0.48	0.12
B	0.0262	-0.0226	0.03	0.33	0.08
C	-0.3907	-0.2718	0.48	4.46	1.15
D	-0.2799	0.5015	0.57	5.38	1.39
E	-0.0093	0.1353	0.14	1.27	0.33
F	-0.1188	-0.0305	0.12	1.15	0.30
G	-0.0454	-0.0522	0.07	0.65	0.17
H	0.0842	0.0395	0.09	0.87	0.22

*The uncertainties are much smaller than the uncertainty of the GC's centre, assumed to be exactly where indicated in Fig. 3, except for the case of NGC 6440G. The 1σ error for the latter are $\theta_\alpha = 0.021$ arcmin and $\theta_\delta = 0.019$ arcmin.

temperature $T_{\rm atm\,+\,spill}$ ($\sim$4.5 K at 45° elevation[17]), the receiver temperature $T_{\rm rec}$ (18 K), the cold sky temperature $T_{\rm sky}$ ($\sim$3.5 K at 1.3 GHz), and the gain of the telescope $G = 2.59\,{\rm K\,Jy^{-1}}$ (for the MeerKAT array observations using 59 antennas). To account for the various sensitivity losses due to signal processing and digitization, we assumed a correction factor of 1.1. NGC 6440G has an estimated mean flux density $S_{1284} = 0.012$ mJy and a pseudo-luminosity $L_{1284} = 0.83$ mJy kpc^2, whereas for NGC 6440H, $S_{1284} = 0.020$ mJy and $L_{1284} = 1.43$ mJy kpc^2 (see Table 2). The results were determined using the integrated pulse profiles shown in the top panels from Fig. 7, obtained by summing together (without including weights) a total of 58 h of observation for both NGC 6440G and NGC 6440H, equivalent to all MeerTime observations that resulted in a detection. For comparison, the 1950-MHz flux densities and their pseudo-luminosities were also obtained using the GBT data and the $T_{\rm sys}$, the gain of the telescope, the BW and the correction factor specified in Freire et al. (2008). The average pulse profiles used in this case are shown in the bottom panels from Fig. 7, obtained by adding all observations made with Spigot, equivalent to 20 h of observation for NGC 6440G. In the case of NGC 6440H, we summed together all the GUPPI observations dedispersed at 1950 MHz, summing a total of 40 h. We did not include weights in any of the cases. The estimated mean flux density of NGC 6440G at 1950 MHz $S_{1950} = 0.006$ mJy and the pseudo-luminosity $L_{1950} = 0.40$ mJy kpc^2, whereas for NGC 6440H, $S_{1950} = 0.009$ mJy and $L_{1950} = 0.60$ mJy kpc^2.

4.4.1 Profile widths

To measure the observed pulse width at 50 per cent of the peak intensity (W50) we again used the template we formed to perform
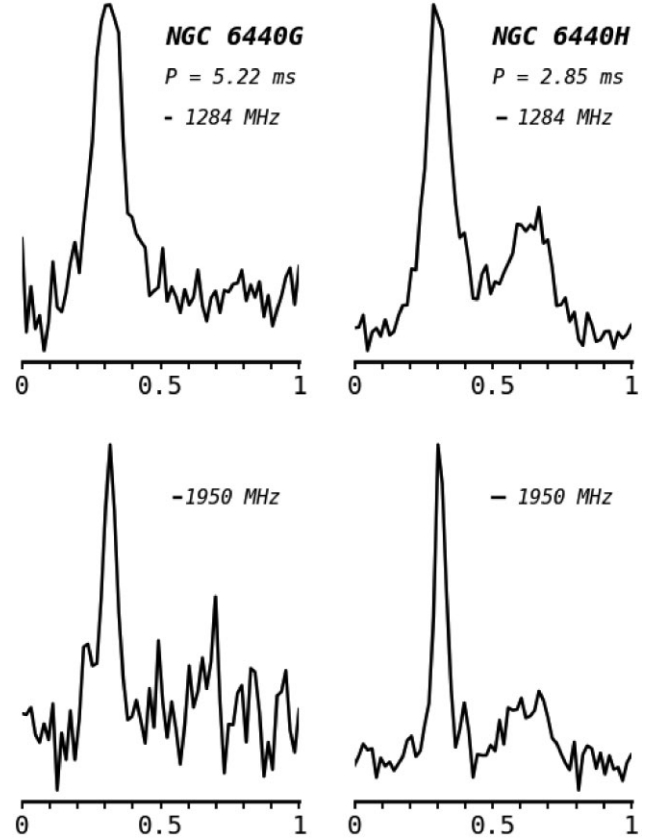
Figure 7. Integrated pulse profiles for the newly discovered pulsars presented here using both L-band (1284 MHz) and S-band (1950 MHz) data from MeerKAT and GBT, respectively. All profiles show one full rotation of the pulsar with 64 phase bins. Their spin periods are indicated. The width of the horizontal bar indicates the effective time resolution of the system, relative to each pulsar's spin period.

the timing analysis. Using the concentration parameter from the best-fitting combination of von Mises functions one can determine the pulse width using the `fitvonMises` function from `PSRSALSA` (Weltevrede 2016). To calculate the error on the width, we generated 1000 simulated noise profiles using the off-pulse noise statistics of the average profile and repeated the von Mises fitting, and determined the width in each case. The error was then estimated from the distribution of width values. The resultant widths are, at 1284 MHz, for NGC 6440G W50 $= (6.31 \pm 0.36) \times 10^{-4}$ s, while for NGC 6440H W50 $= (2.85 \pm 0.10) \times 10^{-4}$ s, which corresponds to a duty cycle of 12 and 10 per cent, respectively. Whereas at 1950 MHz, for NGC 6440G W50 $= (3.05 \pm 0.76) \times 10^{-4}$ s while for NGC 6440H W50 $= (1.40 \pm 0.04) \times 10^{-4}$ s, which corresponds to a duty cycle of 6 and 5 per cent, respectively.

[17]https://skaafrica.atlassian.net/rest/servicedesk/knowledgebase/latest/articles/view/277315585

4.5 High-cadence data analysis for NGC 6440C and NGC 6440D

Previous works (e.g. Bégin 2006; Freire et al. 2008) have presented interesting systematics with time that could be explained by the presence of unmodelled planetary companions (e.g. Cordes 1993). The high-cadence and high-sensitivity MeerTime data provided us an opportunity to detect, or place tight constraints on the presence of planets around NGC 6440C. Similarly, these data and the wide BW of the L-band receiver allowed us to study the eclipses of NGC 6440D in more detail. In this section, we present the results of these analyses.

4.5.1 NGC 6440C

We know that any unmodelled pulsar companions, depending on their mass, may produce orbital effects that can be identified in the timing residuals. NGC 6440C is an apparently isolated MSP with a spin period of 6.23 ms. With the aim of investigating the nature of the systematics in the timing behaviour, we carried out searches for planets using a code which is based on ENTERPRISE[18] (Enhanced Numerical Toolbox Enabling a Robust PulsaR Inference SuitE; Ellis et al. 2020). It uses the Markov chain Monte Carlo technique to fit for the parameters of planets like their period, mass, the white noise and the red noise, among others, using the timing solution of the pulsar (Niţu et al. 2022). We tried different period and mass ranges that were obtained by looking for the maximum amplitude sine wave that can be hidden in the residuals and the minimum amplitude sine wave we might expect based on the ToA errors. These limits are used as input to the mass function equation:

$$f(M_p) = \frac{(M_c \sin i)^3}{(M_p + M_c)^2} = \frac{4\pi^2}{T_\odot} \frac{x^3}{P_b^2}, \qquad (7)$$

where the constant $T_\odot = GM_\odot/c^3 = 4.925\,\mu s$ is used to express the masses in solar units. The red noise was not included in the fit.

We first use the ephemeris from the timing solution obtained using 1 TOA for each of the 26 MeerTime detections, resulting in a data span of 42 d. We did not initially use the TRAPUM data since we first focused on the high-cadence data. For orbital periods ranging between 5 and 35 d, and masses between 1×10^{-3} to $10\,M_\oplus$, our analysis does not find any evidence for planets.

We then expanded the data set by adding all the GBT and TRAPUM data available for this source. With this, we obtained a long-term timing solution over 16 yr. As an example of what is seen in the data, we calculated the Generalized Lomb–Scargle periodogram (Lomb 1976; Scargle 1982) using `cholSpectra` from TEMPO2. From the plot shown in Fig. 8, we see a peak at 23.84 d but it is only $\sim 1.3\sigma$; inspection of the residuals shows that there is some structure on those time-scales, but the signal is clearly weak. We note that this is close to the value of 21.627 d reported by Bégin (2006).

We did the same planetary search using ENTERPRISE and the dynesty sampler fitting for a planet with period between 5 and 35 d and mass between 1×10^{-3} and $10\,M_\oplus$. This fit revealed the possibility of two planets orbiting NGC 6440C, i.e. two different periodicities in the data, so more investigation was warranted. The GBT data were split into two segments of equal number of TOAs. The fits for the first half gave a period of ~ 18.4 d, while the second half showed a period of ~ 36.2 d, two periodicities that are not actually harmonically related. Fig. 9 shows the long-term timing residuals of
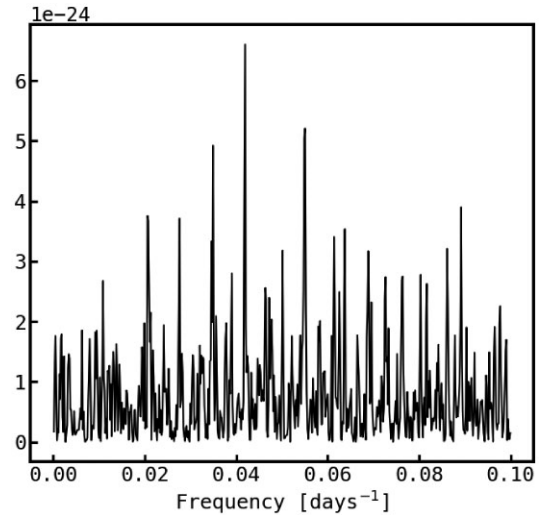
Figure 8. Generalized Lomb–Scargle calculated from the timing residuals from the best-fitting timing solution to the NGC 6440C 16-yr data set, obtained using `cholSpectra` from TEMPO2.
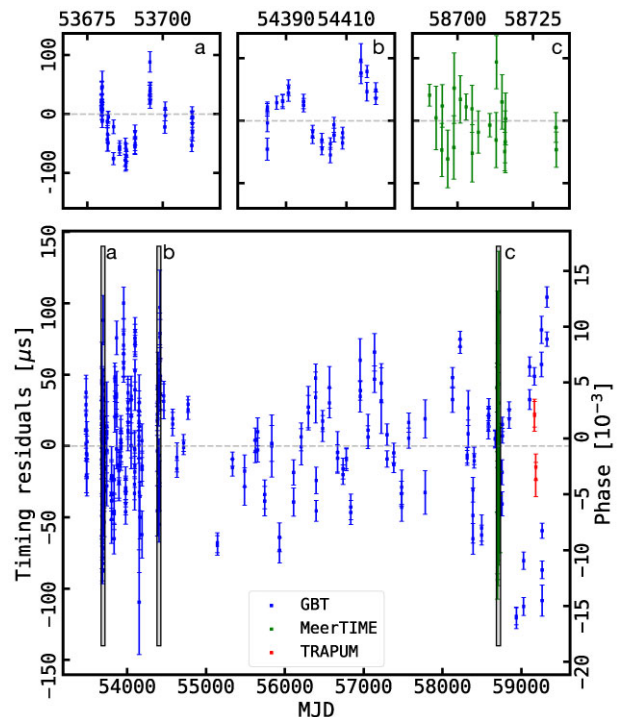

Figure 9. Timing residuals of NGC 6440C as a function of time for GBT and MeerKAT data. The top panels correspond to zoom-in portions of the rectangles labelled as (a), (b), and (c) in the main panel.

NGC 6440C as function of time for GBT and MeerKAT data. If we only consider the infrequent observations over the total observation span, it appears that there is excess white noise in the data. However, the high-cadence observations shown in the inset panels of Fig. 9 show that the noise is correlated on time-scales of tens of days. Correlated noise in pulsars typically takes the form of a red noise process, but here we see no long time-scale fluctuations. Given that correlated structures in three sessions of high-cadence observations with the GBT (panels a and b in Fig. 9) and MeerKAT (panel c in Fig. 9) are not consistent with a purely periodic behaviour, we
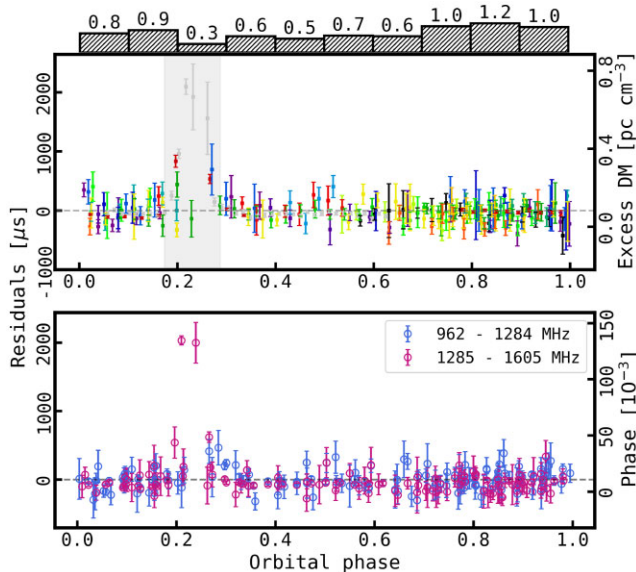
Figure 10. Top panel: Timing residuals and excess DM for the eclipsing binary pulsar NGC 6440D as a function of orbital phase using the frequency range 962–1605 MHz. The eclipse region is highlighted with a grey coloured region. The different epochs are denoted by different colours. The histogram at the top shows a density of ToAs that is not uniform which is related to the timing of the observations. Bottom panel: Variation of timing residuals and phase with orbital phase measured simultaneously in two subbands: 962–1284 MHz (blue circles) and 1285–1605 MHz (pink circles).

suggest that this pulsar exhibits some kind of band-limited noise, or a weekly quasi-periodic process. This might imply association with slow changes in the pulse profile, and hence correlated phase jitter, rather than fluctuations in the spin-down rate typically associated with timing noise. We leave the study of the pulse shape for future work. We note that other pulsars in the cluster observed in the same programmes do not show this excess noise and hence it is unlikely to be related to instrumentation or an artefact of the observing cadence.

4.5.2 NGC 6440D

Taking advantage of the sensitivity and wide band of MeerKAT, we study the eclipses of the Redback NGC 6440D in more detail than previous works (Bégin 2006; Freire et al. 2008). Our data set consists of 18 epochs of observations at the central frequency of 1284 MHz. The timing solution of these observations gave us an orbital period $P_b = 0.286068574(2)$ d and a projected semimajor axis of $x = 0.39722(1)$ lt-s. Delays of ~ 1 ms in the TOA can be seen before, after, and sometimes through the eclipse. The maximum delay in timing residuals around eclipse transitions is ~ 2 ms at ~ 0.22 in phase as visible in the top panel of Fig. 10. The variation in the excess DM with orbital phase derived from the best-fitting timing residuals is also shown in this figure. The presence of an additional electron column density in the eclipse region implied by this dispersive delay, that is, the maximum added electron density near superior conjunction, is found to be $N_{e,\,\mathrm{max}} \geq 2.13 \times 10^{18}$ cm^{-2}. We estimate the corresponding electron density in the eclipse region ($n_e \sim N_e/2a$, where $a = a_p + a_c \approx 2.1$ R$_\odot$, assuming an inclination $i = 90$ deg) as 8.0×10^8 cm^{-3}. The eclipse ingress and egress transitions are spread over a range of orbital phases. The ingress transition starts at orbital phase ~ 0.17, while the eclipse egress ends at ~ 0.29, giving a total span of the eclipse of approximately 12 per cent of the orbit.

Using the mass function from timing $f(m_p, m_c) = 8.2233(7) \times 10^{-4}$ M$_\odot$ and assuming a pulsar mass $m_p = 1.4$ M$_\odot$ and inclination angle $i = 90°$, we obtain a minimum companion mass $m_c = 0.12$ M$_\odot$. The separation of the binary components corresponds to an eclipsing region with physical size of $R_E \sim 0.8$ R$_\odot$, which is larger than the Roche lobe radius of the companion $R_L \simeq 0.5$ R$_\odot$, indicating that the eclipsing material is not gravitationally bound to the companion and that the companion is losing mass (Freire 2005). We also calculate the energy density of the pulsar wind at the companion distance, $U_E = \dot{E}/4\pi^2 c a^2$, and obtain $U_E = 2.50$ erg cm^{-3} using the $\dot{P}$ from Freire et al. (2008) since our $\dot{P}$ estimation would be biased due to the short-term solution. In Fig. 10, we notice that the number of ToAs is significantly less around superior conjunction compared to other orbital phases and an increase of ToAs is seen after inferior conjunction with a maximum density of ToAs at orbital phases 0.7–0.9. We attribute the excess at inferior conjunction to the way the observations were taken, as they were optimized for studying NGC 6440B, with ~ 60 per cent of the observations covering the orbital phases among 0.6 and 1.

In order to study the frequency dependence of the eclipse of NGC 6440D, we divided the observed BW (643 MHz) into two sub-bands as seen in the bottom panel of Fig. 10. The maximum delay in timing residuals around eclipse transitions is ~ 2 ms at ~ 0.22 in phase, this is seen only at higher frequencies (1284–1605 MHz, pink colour in Fig. 10). On the contrary, at lower frequencies (962–1283 MHz, blue colour in Fig. 10), we see a full eclipse. We also observe a larger eclipse duration at the lower frequency band (~ 1.2 times longer for the 962–1283 MHz band than in the 1284–1605 MHz band). We note a longer egress in the 962–1283 MHz band compared to the 1284–1605 MHz band in which case the egress is very quick. The eclipse egress duration at lower frequencies is 23.61 ± 2.54 min. Different ingress/egress duration that depend on the frequency have also been observed for other spider pulsars (e.g. Kudale et al. 2020; Polzin et al. 2020).

5 DISCUSSION

This paper has presented two new MSPs and an analysis of timing data for two of the known pulsars in NGC 6440. The following section will discuss the implications of the results obtained for each of the pulsars studied in this work and examine what the pulsars tell us about the cluster.

NGC 6440G was found to be an isolated pulsar, it has a positional overlap with the X-ray source CX 7 from Pooley et al. (2002) which is proposed as a quiescent LMXB by the authors. The X-ray luminosity of the possible associated source implies a period derivative of the pulsar of the order of $\sim 10^{-19}$ s s^{-1}, a typical value for the MSP population. It is then consistent with the possibility of the association of the source CX 7 with NGC 6440G. However, since the $\dot{P}_{\mathrm{obs}}$ value we have is contaminated by the gravitational potential of the cluster, we cannot confirm the association between the sources. If indeed CX 7 is a qLMXB then the two sources cannot be associated.

Many of the low-mass systems are either Black Widows or Redbacks and they exhibit eclipses. The NGC 6440H 1284-MHz ToAs are well described by a circular orbit and do not show eclipses around superior conjunction. Pulsars with similar characteristics (short orbital period, low-mass companion, and no eclipses) can be found in GCs, e.g. 47 Tuc I, 47 Tuc P, M62 F (Lynch et al. 2012), and NGC 6544A which also has a companion with planetary mass ($M_c \sim 10\,M_J$; D'Amico et al. 2001). The 90 per cent confidence upper limit on the companion mass for NGC 6440H was determined by assuming an inclination angle of $26°$. With this, we find an upper

limit on the companion mass of $\sim 14\,M_J$. The nature of the companion could possibly be explained as an ultra-low-mass carbon white dwarf or a brown dwarf.

There are 57 known pulsars with ultra-light mass companions ($M_{c,min} < 0.08\,M_\odot$) and only nine pulsars[19] with minimum companion masses smaller than $0.01\,M_\odot$ (Manchester et al. 2005). The pulsars with the lightest companions are PSR J2322–2650, with a minimum companion mass of $0.0007\,M_\odot$ ($0.7\,M_J$; Spiewak et al. 2018), and the 'diamond planet' orbiting PSR J1719–1438 with $M_{c,min} = 0.0011\,M_\odot$ ($1.2\,M_J$; Bailes et al. 2011). The minimum companion mass of NGC 6440H makes it the third lowest among all known pulsars[20] and the lowest minimum companion mass in a GC[21] with $M_{c,min} \sim 6.6\,M_J$. B1620–26 is another pulsar with a planetary mass companion located in a GC, M4. It is in a triple system with one companion of a few M_J in a many year orbit which was most likely captured (see e.g. Thorsett et al. 1999; Sigurdsson et al. 2003, 2008).

The fact that both NGC 6440G and NGC 6440H were missed in the GBT data was expected, since they are very faint even after folding with a precise ephemeris (see Section 4.4). The archival GBT data can recover the signal from the pulsars only after the orbits were first characterized in the MeerKAT observations, decreasing acutely the number of trials necessary for a detection. With this, a suitable set of ToAs can be determined. These can be then used to derive a long-term timing solution with precise timing parameters.

The structure in the timing residuals of NGC 6440C are not well modelled as a standard power-law-like noise process but are also not modelled by a planet, or planets. The quasi-periodic nature of the variations argues against them being due to random dynamical interactions with passing stars. So the origin of the unusual variations in arrival times is unclear and probably requires a dedicated long term and high-cadence, high-sensitivity observing campaign to better constrain the properties and hence the origin.

The detection of NGC 6440D at higher frequencies during the eclipse phase indicates an orbital inclination that is likely less than $90°$ and it implies a highly variable concentration of eclipsing material. This has also been seen in other similar systems. Moreover, the longer egress duration at lower frequencies suggest that the companion's orbital motion causes its wind to be swept back (Fruchter et al. 1990; Stappers et al. 2001) leaving a cometary-like tail of material (Main et al. 2018) causing the eclipses to be extended. At higher frequencies typical pulse smearing effects like scattering or dispersion would be less prominent. Since the eclipse is not always total (see Fig. 10) the eclipse could be caused by grazing incidence of the pulsar beam on a wind from the companion.

Comparing the values of the eclipse radius, Roche lobe radius, orbital period P_b, energy density of pulsar wind at the companion distance U_E and $N_{e,max}$ for NGC 6440D with those of other eclipsing Redback pulsars from the Galaxy, we find that this MSP is similar in most respects (see Polzin et al. 2020). This pulsar is far away from the cluster centre and its period derivative is not highly affected by the gravitational potential of the cluster.

Besides the eight pulsars (NGC 6440A-H), this cluster also hosts seven probable quiescent LMXBs (Heinke et al. 2003) and it was the first cluster in which two luminous transient LMXBs were found (both showing millisecond pulsations; Heinke et al. 2010). A third

transient X-ray binary was recently found in Terzan 5 (Bahramian et al. 2014). NGC 6440 has a relatively high interaction rate per binary, $\gamma \propto \rho_c/\nu$, ρ_c is the density of the cluster, and ν is the velocity dispersion. Terzan 5 and NGC 6440 are among the most massive and densest clusters of the non-core collapsed GCs (see table 1 from Verbunt & Freire 2014). These clusters with 'intermediate' γ are expected to host a mix of isolated and binary pulsars, like in the case of NGC 6440 with the exact same number of isolated and binary pulsars known to date. The peculiarity of NGC 6440 is its large production of binary systems with low-mass companions. This can be understood primarily as a consequence of the high density of the cluster and the large γ value for a non-core-collapsed cluster. Krolik, Meiksin & Joss (1984) suggest that in clusters with high-central density isolated NSs or NSs with a very low mass companions are produced by direct collision between main-sequence stars and NSs. Also, Ivanova et al. (2008) find that the formation of LMXBs has a 50 per cent contribution by binary exchange, physical collisions with giants and tidal capture in high density clusters. Additionally, in these clusters with intermediate or high encounter rates per binary, the formation of a new LMXB system could be possible via 'secondary' exchange encounters as a result of an already recycled pulsar acquiring a main-sequence star companion (Verbunt & Freire 2014).

NGC 6440 has the characteristics one would expect for a GC with an intermediate to high γ: there is an apparently young pulsar, NGC 6440A, with a characteristic age $\sim 10^3$ times smaller than the age of the cluster, there is one binary system with a high eccentricity (similar to what is seen in clusters like Terzan 5 and M28), it also hosts two pulsars that lie more than four core radius from the centre, NGC 6440C and NGC 6440D. But no pulsars have been found further than the half-mass radius, like in the case of other core-collapsed clusters (e.g. NGC 6752; D'Amico et al. 2002; Corongiu et al. 2006). For all these reasons, it is not surprising that the pulsar with the lightest companion known so far in a GC is found in this cluster. It is important to note that although Terzan 5 and NGC 6440 have approximately the same encounter rate and the same encounter per binary rate, they have different pulsar populations and the particular internal distribution of spin periods is different. The past dynamical history of the cluster must have had some influence on these.

6 CONCLUSIONS

Two new pulsars have been discovered in NGC 6440 using MeerKAT: one of them is isolated, NGC 6440G, and the other one, NGC 6440H, is a Black widow which does not display eclipses in the 962–1605 MHz band. The companion to NGC 6440H is also the lightest mass pulsar companion so far known in a GC, with a minimum mass of $0.006\,M_\odot$. The two new additions maintain the previously observed equal ratio of isolated and binary pulsars in NGC 6440 (now 4:4), and contributes to the pulsar discoveries in GCs using MeerKAT.

The high-cadence of the complementary MeerTime and TRAPUM observations, as well as the large BW of MeerKAT also enabled us to study in detail the known pulsars NGC 6440C and NGC 6440D. On the basis of the new data, we could reject the existence of planets in simple configurations around the isolated pulsar NGC 6440C. Further studies of the profile variability are warranted to gather more information about the systematics found in the timing residuals of this pulsar. Our analysis of the eclipses of the Redback pulsar NGC 6440D at two different frequency bands revealed a clear frequency dependence, with longer and asymmetric eclipses occurring at the lower frequencies (962–1283 MHz).

---

[19]This number does not include pulsar B1620–26 since the mass of planetary companion is not well known and it is not included in the ATNF catalogue.
[20]https://www.atnf.csiro.au/research/pulsar/psrcat/
[21]See http://www.naic.edu/~pfreire/GCpsr.html.

We note that the precise timing parameters obtained for both NGC 6440G and NGC 6440H would not have been possible without the availability of the archival GBT data that enabled us to derive a ∼15 yr long timing solution. Moreover, the tiling capabilities of the TRAPUM back-end have helped us to obtain a better localization for the very faint and relatively steep spectrum ($\alpha \approx -1.76$) pulsar NGC 6440G and thus improve the timing solution.

Additional observations of NGC 6440 and of a large set of other GCs are being collected as part of the TRAPUM GC pulsar survey, which exploits the full MeerKAT array.

DATA AVAILABILITY

The data that support the findings of this article will be shared on reasonable request to the MeerTime and TRAPUM collaborations.

REFERENCES

Alpar M. A., Cheng A. F., Ruderman M. A., Shaham J., 1982, Nature, 300, 728

Altamirano D. et al., 2010, ApJ, 712, L58

Bahramian A. et al., 2014, ApJ, 780, 127

Bailes M. et al., 2011, Science, 333, 1717

Bailes M. et al., 2020, Publ. Astron. Soc. Aust., 37, e028

Baumgardt H., Hilker M., 2018, MNRAS, 478, 1520

Bégin S., 2006, Master's thesis, University of British Columbia

Bogdanov S., Bahramian A., Heinke C. O., Freire P. C. C., Hessels J. W. T., Ransom S. M., Stairs I. H., 2021, ApJ, 912, 124

Camilo F. et al., 2018, ApJ, 856, 180

Chen W., Barr E., Karuppusamy R., Kramer M., Stappers B., 2021, J. Astron. Instrum., 10, 2150013

Clark G. W., 1975, ApJ, 199, L143

Cordes J. M., 1993, in Phillips J. A., Thorsett S. E., Kulkarni S. R., eds, ASP Conf. Ser. Vol. 36, Planets Around Pulsars. Astron. Soc. Pac., San Francisco. p. 43

Corongiu A., Possenti A., Lyne A. G., Manchester R. N., Camilo F., D'Amico N., Sarkissian J. M., 2006, ApJ, 653, 1417

D'Amico N., Lyne A. G., Manchester R. N., Possenti A., Camilo F., 2001, ApJ, 548, L171

D'Amico N., Possenti A., Fici L., Manchester R. N., Lyne A. G., Camilo F., Sarkissian J., 2002, ApJ, 570, L89

Dewdney P. E., Hall P. J., Schilizzi R. T., Lazio T. J. L. W., 2009, Proc. IEEE, 97, 1482

Dewey R. J., Taylor J. H., Weisberg J. M., Stokes G. H., 1985, ApJ, 294, L25

Douglas A. et al., 2022, ApJ, 927, 126

DuPlain R., Benson J., Sessoms E., 2008a, in Bridger A., Radziwill N. M., eds, Proc. SPIE Conf. Ser. Vol. 7019, Advanced Software and Control for Astronomy II. SPIE, Bellingham, p. 70191A

DuPlain R., Ransom S., Demorest P., Brandt P., Ford J., Shelton A. L., 2008b, in Bridger A., Radziwill N. M., eds, Proc. SPIE Conf. Ser. Vol. 7019, Advanced Software and Control for Astronomy II. SPIE, Bellingham, p. 70191D

Ellis J. A., Vallisneri M., Taylor S. R., Baker P. T., 2020, ENTERPRISE: Enhanced Numerical Toolbox Enabling a Robust PulsaR Inference SuitE, Zenodo. Available at: https://doi.org/10.5281/zenodo.4059815

Folkner W. M., Williams J. G., Boggs D. H., 2009, Interplanetary Network Progress Report, 42–178, 1

Freire P. C. C., 2005, in Rasio F. A., Stairs I. H., eds, Proc. SPIE Conf. Ser. Vol. 328, Binary Radio Pulsars. SPIE, Bellingham, p. 405

Freire P. C., Kramer M., Lyne A. G., 2001, MNRAS, 322, 885

Freire P. C. C., Hessels J. W. T., Nice D. J., Ransom S. M., Lorimer D. R., Stairs I. H., 2005, ApJ, 621, 959

Freire P. C. C., Ransom S. M., Bégin S., Stairs I. H., Hessels J. W. T., Frey L. H., Camilo F., 2008, ApJ, 675, 670

Fruchter A. S. et al., 1990, ApJ, 351, 642

Gavriil F. P., Strohmayer T. E., Swank J. H., Markwardt C. B., 2006, in AAS/High Energy Astrophysics Division #9, p. 1.43

Gavriil F. P., Strohmayer T. E., Swank J. H., Markwardt C. B., 2007, ApJ, 669, L29

Heinke C. O., Grindlay J. E., Lugger P. M., Cohn H. N., Edmonds P. D., Lloyd D. A., Cool A. M., 2003, ApJ, 598, 501

Heinke C. O. et al., 2010, ApJ, 714, 894

Hobbs G., Edwards R., Manchester R., 2006, Chin. J. Astron. Astrophys. Suppl., 6, 189

Hotan A. W., van Straten W., Manchester R. N., 2004, Publ. Astron. Soc. Aust., 21, 302

Ivanova N., Heinke C. O., Rasio F. A., Belczynski K., Fregeau J. M., 2008, MNRAS, 386, 553

Kaplan D. L. et al., 2005, PASP, 117, 643

Katz J. I., 1975, Nature, 253, 698

King I., 1962, AJ, 67, 471

Kramer M. et al., 2021, MNRAS, 504, 2094

Krolik J. H., Meiksin A., Joss P. C., 1984, ApJ, 282, 466

Kudale S., Roy J., Bhattacharyya B., Stappers B., Chengalur J., 2020, ApJ, 900, 194

Lazaridis K. et al., 2009, MNRAS, 400, 805

Lomb N. R., 1976, Ap&SS, 39, 447

Lynch R. S., Freire P. C. C., Ransom S. M., Jacoby B. A., 2012, ApJ, 745, 109

Lyne A. G., Brinklow A., Middleditch J., Kulkarni S. R., Backer D. C., 1987, Nature, 328, 399

Lyne A. G., Manchester R. N., D'Amico N., 1996, ApJ, 460, L41

Main R. et al., 2018, Nature, 557, 522

Manchester R. N., Hobbs G. B., Teoh A., Hobbs M., 2005, AJ, 129, 1993

Nice D. J., Taylor J. H., 1995, ApJ, 441, 429

Niţu I. C., Keith M. J., Stappers B. W., Lyne A. G., Mickaliger M. B., 2022, MNRAS, 512, 2446

Origlia L., Valenti E., Rich R. M., 2008, MNRAS, 388, 1419

Ortolani S., Barbuy B., Bica E., 1994, A&AS, 108, 653

Pallanca C. et al., 2021, ApJ, 913, 137

Pan Z. et al., 2020, ApJ, 892, L6

Pan Z. et al., 2021, ApJ, 915, L28

Phinney E. S., 1992, Phil. Trans. R. Soc. A, 341, 39

Polzin E. J., Breton R. P., Bhattacharyya B., Scholte D., Sobey C., Stappers B. W., 2020, MNRAS, 494, 2948

Pooley D. et al., 2002, ApJ, 573, 184

Radhakrishnan V., Srinivasan G., 1982, Curr. Sci., 51, 1096

Ransom S. M., 2008, in Vesperini E., Giersz M., Sills A., eds, Proc. IAU Symp. 246, Dynamical Evolution of Dense Stellar Systems. Cambridge Univ. Press, Cambridge, p. 291

Ransom S. M., Eikenberry S. S., Middleditch J., 2002, AJ, 124, 1788

Ransom S. M., Cordes J. M., Eikenberry S. S., 2003, ApJ, 589, 911

Ridolfi A. et al., 2021, MNRAS, 504, 1407

Ridolfi A. et al., 2022, MNRAS, preprint (arXiv:2203.12302)

Scargle J. D., 1982, ApJ, 263, 835

Shklovskii I. S., 1970, SvA, 13, 562

Sigurdsson S., Richer H. B., Hansen B. M., Stairs I. H., Thorsett S. E., 2003, Science, 301, 193

Sigurdsson S., Stairs I. H., Moody K., Arzoumanian K. M. Z., Thorsett S. E., 2008, in Fischer D., Rasio F. A., Thorsett S. E., Wolszczan A., eds, ASP Conf. Ser. Vol. 398, Extreme Solar Systems. Astron. Soc. Pac., San Francisco, p. 119

Spiewak R. et al., 2018, MNRAS, 475, 469

Stappers B., Kramer M., 2016, Proc. Sci., MeerKAT Science: On the Pathway to the SKA. SISSA, Trieste, PoS#009

Stappers B. W., Bailes M., Lyne A. G., Camilo F., Manchester R. N., Sandhu J. S., Toscano M., Bell J. F., 2001, MNRAS, 321, 576

Thorsett S. E., Arzoumanian Z., Camilo F., Lyne A. G., 1999, ApJ, 523, 763

Trager S. C., Djorgovski S., King I. R., 1993, in Djorgovski S. G., Meylan G., eds, ASP Conf. Ser. Vol. 50, Structure and Dynamics of Globular Clusters. Astron. Soc. Pac., San Francisco, p. 347

Valenti E., Ferraro F. R., Origlia L., 2007, AJ, 133, 1287

van Straten W., Bailes M., 2011, Publ. Astron. Soc. Aust., 28, 1

van Straten W., Demorest P., Oslowski S., 2012, Astron. Res. Technol., 9, 237

Verbunt F., Freire P. C. C., 2014, A&A, 561, A11

Verbunt F., Kuiper L., Belloni T., Johnston H. M., de Bruyn A. G., Hermsen W., van der Klis M., 1996, A&A, 311, L9

Vitral E., 2021, MNRAS, 504, 1355

Wang L. et al., 2020, ApJ, 892, 43

Webbink R. F., 1985, in Goodman J., Hut P., eds, Proc. IAU Symp. 113, Dynamics of Star Clusters. Reidel, Dordrecht, p. 541

Weltevrede P., 2016, A&A, 590, A109

This paper has been typeset from a TeX/LaTeX file prepared by the author.